Superhydrophobicity Transfer Effect in Superwetting Coatings for Strengthening Anti-pollution Flashover Performance

Chuxiong Qiu[a], Wei Xiong[a], Helong Zhang[a], Rong Zhang[a], Ivan P. Parkin[b], Shengwu Wang[c], Lee Li[c], Junwu Chen[c], Zhi Chen[c], Arnauld Robert Tapa[a,d], Albert Trokourey[d], Weibing Zhou[a], Xiujian Zhao[a], Yi Xie[a,*]

[a] State Key Laboratory of Silicate Materials for Architectures, Wuhan University of Technology, No. 122, Luoshi Road, Wuhan 430070, P. R. China

[b] Department of Chemistry, University College London, London WC1H 0AJ, U.K.

[c] School of Electrical and Electronic Engineering, Huazhong University of Science and Technology (HUST), Wuhan 430074, China

[d] Félix Houphouët-BOIGNY University, Constitution and Reaction of Matter Laboratory, Côte d'Ivoire

ABSTRACT

Superhydrophobic (SH) and superamphiphobic (SAP) coatings have been viewed as an alternative to conventional hydrophobic room temperature vulcanizing (RTV) silicone rubber coatings in anti-pollution flashover application. However, being one of the most important properties in RTV-based anti-flashover materials and devices, the hydrophobicity transfer property was rarely documented for SH and SAP coatings, which restricts their practical applications in environments with heavy contamination. Herein, we propose for the first time a superhydrophobicity transfer effect in superwetting (SW) coatings (e.g., SAP and SH coatings) containing low-surface-energy molecules (e.g., polydimethylsiloxane (PDMS)) as a migratory reagent. When the surface is stained by artificial simulated pollutants, PDMS molecules can migrate from the coating to the contamination layer, followed by a surface modification. Through this process, the surface wettability of the contaminant layer gradually evolves from superhydrophilicity to hydrophobicity, and finally to SH state. This evolution is investigated in relation to the amount of PDMS, migration time, pollution grade, and pollutant species. The superhydrophobicity transfer effect offers the coated glass insulators an outstanding anti-pollution flashover strength. This work can provide a novel and universal protocol to realize a superhydrophobicity transfer property in SW coatings, which may stimulate further investigation and applications in not only anti-pollution flashover but also other fields such as anti-fouling and anti-icing.

Keywords:

Superhydrophobic coatings; superamphiphobic coatings; superhydrophobicity transfer effect; anti-pollution flashover; flashover voltage

1. Introduction

Superwetting (SW) surfaces that mimic biological systems, such as superhydrophobic (SH) and superamphiphobic (SAP) surfaces, have opened up new research vistas and found wide-ranging applications in a variety of fields, such as anti-fogging [1], anti-icing [2-5], antibacterial [6], oil-water separation [7], anti-reflection for photovoltaics [8], stabilizing water-sensitive luminescent nanomaterial [9], and anti-corrosion [10-13]. Recently, due to their exceptional anti-pollution and insulating performances, SH materials have attracted great attention in external insulation system of power transmission lines [14, 15]. In particular, SH coatings have been viewed as an alternative to conventional room temperature vulcanizing (RTV) silicone rubber materials for improving flashover strength [16-21]. Fabricating an additional SH coating on intrinsically hydrophilic glass or porcelain insulators can effectively prevent water droplets from adhering to and spreading across the surface, making it easier to solve the pollution issues on the insulators and less likely that a flashover will occur [18, 19, 21-23].

A lot of studies have been carried out on the electrohydropdynamic behavior of water droplets on the SH surfaces and the impact on the surface anti-flashover performance. Li *et al.* noticed that water droplets tended to a self-propelled motion and slide from SH surface under electric field while water tended to elongate and break up on the RTV surface [24]. The droplet sliding behavior is due to the low adhesion between the water and the SH surface and a sufficiently high electrostatic force provided by the DC voltage, which resulted to an elevated flashover voltage compared with that of the ordinary RTV [17]. The rolling away of water droplets driven by the electrical field force can remove water-insoluble pollution particles [25], alleviating the electrical distortion caused by the droplets and consequently elevating the wet flashover voltage of coated silicone rubber by 60% in comparison with that of pristine silicone rubber [26].

Effective efforts through fabricating SH surfaces to enhance the flashover performances of coatings and electrical devices in the power system have been made. For instance, compared with the RTV and untreated

glass insulator strings, the SH insulator string showed 31% and 150% increased flashover voltages, respectively, under a medium pollution grade [19]. By incorporating inorganic particles into polydimethylsiloxane (PDMS) elastomer solution, the surface flashover strength could be increased by 54% [21]. The superhydrophobicity was capable of enhancing the insulation performance of a coating surface, and thus led to low leakage currents when exposed to high humidity conditions [27, 28]. We have also confirmed that at any pollution degree, the leakage current of the SH surface was always much smaller than that of the RTV and uncoated surfaces [18]. Further study indicated that the increase of pollution degree led to the reduction of flashover voltage, and the reduction in the case with SH coating was smaller than that with RTV coating [20]. Comparatively, despite that SAP coatings has shown wide applications in lots of fields, its potential in anti-pollution flashover was rarely reported. Very recently, we developed a facile protocol to fabricate SAP coating with unique gradient and hierarchical architecture, and explored the excellent anti-flashover performances of the as-deposited coatings on glass insulators [22].

It's worth noting that although SH coatings have strong water repellency, during long-term running in severe environment with heavy pollution, contaminants may build on the surface. The presence of the hydrophilic contaminants will lead to the reduction or loss of the hydrophobicity of the original surfaces. Furthermore, the pollution flashover voltage on SH coatings is affected by the distribution characteristics of surface pollution [29, 30]. Therefore, it is critical to offer the SH coatings the hydrophobicity transfer capability by analogy to that of RTV- coatings. In RTV system, when the surface is covered by hydrophilic contaminants, hydrophobic species can migrate from RTV to the contamination layer, gradually turning the wettability of contamination layer from hydrophilicity to hydrophobicity [31]. This particular characteristic is essential for reducing partial discharge and leakage currents of anti-pollution flashover materials in severely contaminated environments. Recently, the preliminary exploration on the hydrophobicity transfer in SH coatings has been conducted [32, 33]. However, the hydrophobicity transfer ability was still poor. Furthermore, the composition of the transferring species was not exactly identified and elucidated.

Consequently, it is crucial to deepen the inquiry into the hydrophobicity transfer performance in SH and SAP coatings and to unambiguously clarify the underlying mechanism.

Herein, we developed a facile and general approach to realize a unique superhydrophobicity transfer property in SW coatings (Scheme 1). Typically, the SH and SAP coatings were fabricated by modifying a recently published procedure [22], except that low-surface-energy migratory organic species (e.g., PDMS, polymethylhydrosiloxane) is introduced to the coating (mainly primer). When the surface was contaminated by artificial pollution layers (e.g., diatomite, fly ash, kaolin, cement ash, and a mixture of diatomite and NaCl), the embedded low-surface-energy molecules can migrate from the primer to the pollution layer, leading to a progressive evolution of the pollution layer's wettability from superhydrophilicity to superhydrophobicity. We refer to this particular property as superhydrophobicity transfer effect, analogous to the hydrophobicity transfer in the widely-reported RTV system. The influence of the amount of migratory reagent, migration time, the pollution type and grade on the superhydrophobicity transfer property is systematically investigated. The mechanism of superhydrophobicity transfer is revealed by the characterizations of the contaminant layer and the self-healing ability of the SH coating. We finally show that the superhydrophobicity transfer effect can improve the anti-pollution flashover strength of the coated insulators.

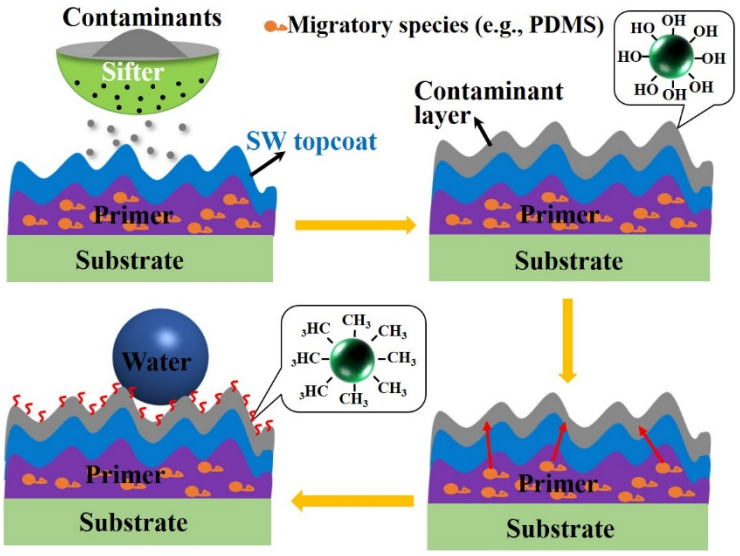

Scheme 1. The schematic diagram illustrating the mechanism of superhydrophobicity transfer effect of the superwetting coating.

2. Experimental

2.1. Chemicals and materials

Hexamethyl disilazane (HMDS, AR), butyl acetate (AR) and NaOH (96.0%) were purchased from Aladdin; ethanol (EtOH, AR) and tetraethyl orthosilicate (TEOS, AR) from Sinopharm Chemical Reagent Co. Ltd. Polydimethylsiloxane (PDMS, with viscosity of 100 ± 8 mPa·s, AR), polymethylhydrosiloxane (PMHS, with viscosity of 15-40 mPa·s, AR), vinyl silicone oil (VES, with viscosity of 90 mPa·s, AR) and 1H, 1H, 2H, 2H-perfluorodecyltrimethoxysilane ($C_{13}H_{12}O_3F_{18}Si$, PFDTMS) were purchased from Macklin; silane coupling agent (KH550) from Suixin Chemical Co. Ltd., Guangzhou; nylon powder (500 #) from DuPont; alkyd resin and polypropylene resin from Yoshida Chemical Co. Ltd., Shenzhen; tetrafluoro resin (HLR-6) from East Fluorochemical Technology Co., Ltd, Shanghai. Kaolin (1250 meshes) was purchased from Shanxi Xingle Kaolin Co. Ltd; fly ash (325 meshes) from Henan Zhengzhou Huifeng New Materials Co. Ltd.; cement ash (strength grade 32.5) from Sichuan Mianzhu Baichuan Special Cement Co. Ltd.; diatomite

(600 meshes) from Hebei Shijiazhuang Dehang Mineral Materials Co. Ltd. The chemicals were used as received without any further purification.

2.2. Preparation of resin-based and silica-based dispersions

The resin-based dispersion, silica nanoparticles (NPs) and their surface modification were achieved by a recently-reported approach [22], except that low-surface-energy migratory organic reagent (e.g., PDMS, PMHS, VES) with varied fractions are introduced in the resin-based dispersion. In the brief preparation of a PDMS-embedded resin-based dispersion, alkyd resin (6.0 g) was dissolved in butyl acetate (30 mL) under stirring, followed by sequentially adding polypropylene resin (1.8 g), tetrafluoro resin (1.0 g), KH550 solution (pre-dissolved 0.22 mL KH550 in 0.32 mL ethanol and 0.06 ml H_2O), nylon particle powder (1.0 g) and PDMS (0.45 g). Herein, tetrafluoro resin and polypropylene were introduced to enhance the resistance to abrasion and the durability of the coatings. The addition of the nylon particles facilitates the formation of mastoid-like microstructure in the primer and the subsequent micro-nano structure after deposition of the topcoat, which plays critical role in the creating SAP and SH surfaces. The above dispersion was kept stirring for an additional 24 h to obtain a well-dispersed resin-based dispersion, which can be used for depositing primer. The detailed synthesis procedure of silica NPs and their surface modification by using PFDTMS and HMDS are provided in the Supporting Information (SI).

2.3. Fabrication of SAP and SH coatings

The SAP and SH coatings were obtained by sequentially depositing the resin-based primer and the silica-based topcoat on substrates, under ambient environment (20-30^{o}C, relative humidity ~50-60 %). SAP and SH coatings were deposited by using PFDTMS- and HMDS-modified silica NP dispersions as the topcoat, respectively. Pre-cleaned glass slides and glass insulators (XP-70 with an average diameter of 25.5 cm) were used as substrates. Typically, the resin-based and silica-based suspensions were sequentially spray-deposited onto the substrates using an airbrush with a nozzle diameter of 1.0 mm at a pressure of 2.0-2.5 bar (nozzle to substrate surface distance 15-20 cm). The resin-based primer layer was kept for evaporation

for 2-3 min before spraying the silica-based topcoat. Two and three cycles of spraying were performed for the primer and topcoat, respectively, followed by drying at room temperature (RT).

2.4. Materials characterization

The field emission scanning electron microscopy (FESEM, Hitachi S-4800) was utilized to characterize the surface morphologies of the various coatings. Fourier transform infrared (FTIR, Nicolet 6700, USA) spectra and X-ray photoelectron spectroscopy (XPS, ESCALAB 250Xi, USA) were used to analyze the surface structure and elemental composition of the contaminants before and after superhydrophobicity transfer. The tests of static water contact angle (WCA), water sliding angle (WSA) and oil contact angle (OCA) were performed on an optical contact angle meter (Theta Lite, Biolin Scientific) by sessile drop method at RT, among which bean oil was used for the OCA test. Chemical stability of the coatings was monitored by the evolution of WCAs and WSAs after soaking the coated glass slides in acidic or alkaline solutions for different periods of time, in which the pH values were tuned from 1.0 to 14.0 by using H_2SO_4 and NaOH solutions. The UV stability was investigated by monitoring the evolution of the surface wettability upon illuminating the coatings with a UV lamp (UVA-340, 40 W), by fixing the lamp to coating distance as 20 cm.

2.5. Self-healing of the SH coating

The self-healing ability of the SH coating against oxygen plasma treatment was investigated. The coated SH glass slides were partially exposed to a plasma treatment for 25 s, by covering half of the coated glass slide in a plasma cleaning machine (Hefei Jusheng Vacuum Technology Co., Ltd., P15, 80 W). The plasma-treated coating was transferred to a constant temperature (25^{o}C) and humidity chamber (60 %), and were then subjected to WCA measurements at different periods of time to monitor the evolution of self-healing performance.

2.6. Design and test of superhydrophobicity transfer

Diatomite, fly ash, kaolin, cement ash, and a mixture of diatomite and NaCl (diatomite:NaCl weight ratio of 6:1) were used as simulated artificial contaminants for the test of superhydrophobicity transfer effect. The surface contamination was performed by a sieving method since the SH and SAP surfaces were very difficult to be contaminated by brushing artificial pollution slurry that has been widely reported in the RTV system [22]. Typically, the contaminants were evenly sieved on the SH or SAP coatings with a 200# sieve to form a hydrophilic pollution layer. Each specimen was placed in the same chamber to keep identical circumstance (25 ± 3°C, relative humidity 50 ± 10%) for superhydrophobicity transfer. After a certain period of time, the pollution particles were carefully collected and flattened on a clean glass slide for the test of WCA, WSA and OCA, based on which the surface wettability evolution of the contaminants over migration time was recorded. If the WCA exceeds 150°, it indicates that the hydrophilic contaminant layer has been converted to superhydrophobic phase due to the migration of low-surface-energy species from the SH or SAP coating to the contaminants layer.

2.7. Flashover test

The pollution flashover tests of the various coated glass insulators were conducted in an artificial flashover platform under a rising AC voltage in atmosphere conditions. A layer of contaminants was evenly sieved on the coated insulators with a 200# sieve and the migration time was kept for 168 h in an ambient environment to complete the superhydrophobicity transfer. Afterwards, the insulators were fully exposed to saturated moisture with an inclination angle of 15° in a fog chamber for 15 min. The applied AC voltage on the specimen was then gradually raised until the flashover occurred, from which the pollution flashover voltage (PFOV) was estimated.

3. Results and Discussion

3.1. Superhydrophobicity transfer property of the hydrophobic PDMS-embedded resin-based coating

In order to fully understand the mechanism underlying the superhydrophobicity transfer effect of the SH and SAP coatings that will be discussed in the following sections, we first present the superhydrophobicity transfer capability of the bare resin-based primer (i.e., without silica-based topcoat) incorporated with different PDMS weight percents (w%). The surface of the representative primer demonstrates a mastoid-like microstructure due to the presence of nylon particles (Fig. 1a-b) and a hydrophobic performance with WCA around 95.6^{o} (inset in Fig. 1a). Superhydrophilic contaminants (e.g., diatomite powder) were sieved on the resin-based primer, and the evolution of the contaminant layer's surface wettability (evaluated by WCAs) during the course of the covering period was monitored. The primer retains its overall surface morphology and hydrophobic performance (see inset in Fig. 1c) after the diatomite powder was removed, except that a very small number of diatomite particles were attached to the surface (Fig. 1c-d). We use migration time to express covering time because, as we will discuss in the following sections, the superhydrophobicity transfer is caused by the migration of low-surface-energy species. As shown in Fig. 1e, the WCA on the contaminant layer grows consistently with the prolonging migration time. In a typical primer with 0.9 w% PDMS, the WCA of the contaminant layer can be increased from ~0^{o} on the fresh contaminants to ~87.6^{o} after 24 h of migration time, and reach 151.1^{o} in 72 h (the red curve in Fig. 1e). As a comparison, no matter how lengthy the migration time is, the diatomite layer collected from a PDMS-absent primer always displayed a WCA below 5^{o} (not shown here). Besides, increasing the PDMS fraction in the primer can significantly shorten the migration time to convert the contaminant layer from superhydrophilicity to SH state. For instance, when the PDMS weight percent is 1.8%, the time for the contaminants to reach a SH state is shortened to 36 h (blue curve in Fig. 1e, WCA = 150.9^{o}); whereas in the case of 0.3 w% PDMS, the corresponding migration time is prolonged to 108 h (see black curve in Fig. 1e). As further confirmed in Fig. 1f, increasing the PDMS fraction in the primer resulted in larger WCAs on the contaminated layer when the migration duration was fixed. Excess PDMS (e.g., over 0.9 w%) changes no much the WCAs once the wettability of the contaminants reaches a SH state.

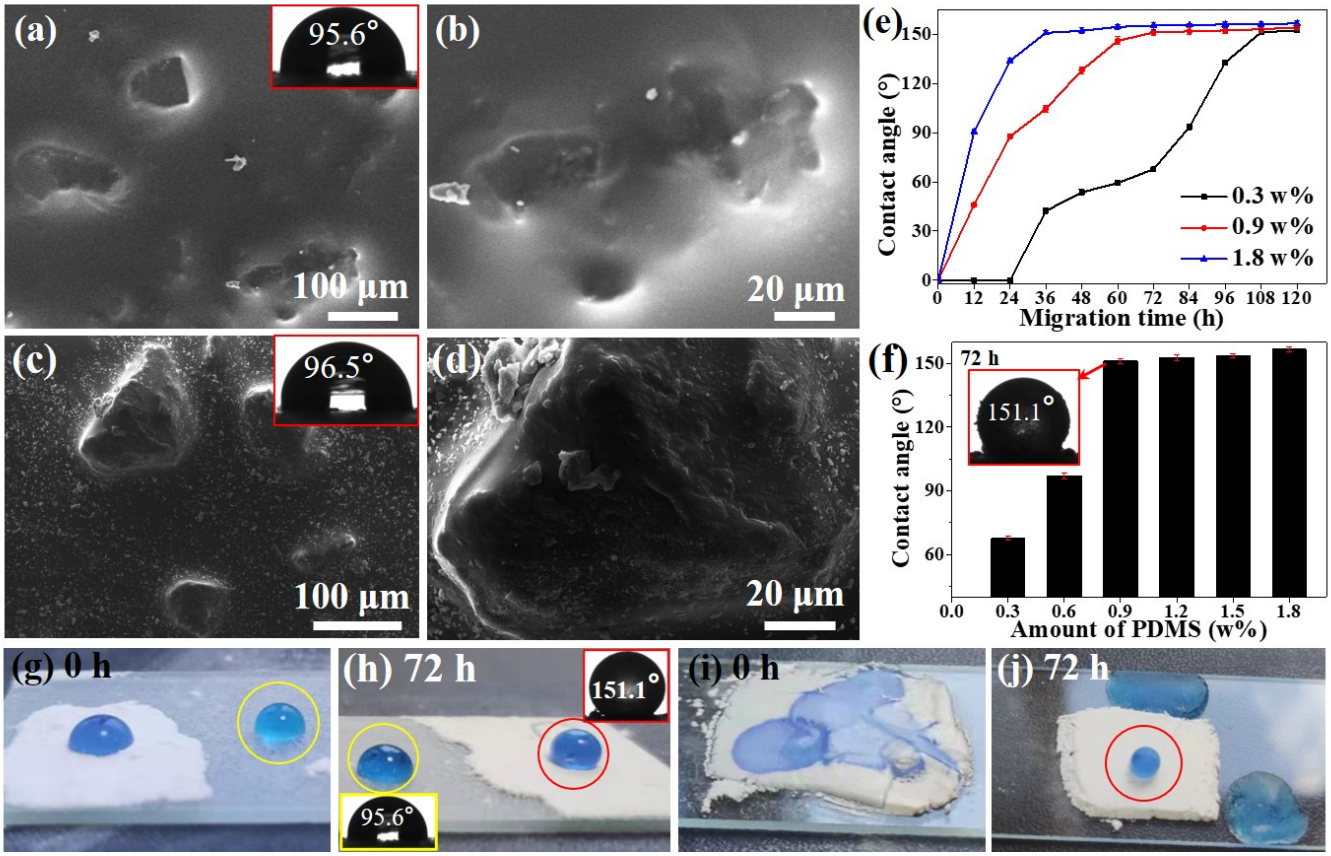

Fig. 1. Characterization and superhydrophobicity transfer performance of the PDMS-embedded resin-based primer. (a-b) SEM images of the primer as-achieved in the presence of 0.9 w% PDMS. (c-d) SEM images of the primer after 72 h of migration time and the contaminants were removed. (e) Evolution of WCAs on the contaminant (i.e., diatomite) layer over migration time, in which the primers were fabricated with different weight percents of PDMS. (f) Evolution of WCAs on the contaminant layers as-removed from a series of primers fabricated with different weight percents of PDMS. The migration time was fixed to 72 h. (g-h) *In-situ* digital photographs of primer partially covered by diatomite layer for 0 h (g) and 72 h (h), respectively, together with dyed water droplets. (i-j) Digital photographs of water droplets and diatomite layer on glass slides, where the diatomite was transferred from the primer after migration of 0 h (i) and 72 h (j), respectively.

The conversion from superhydrophilicity to SH state can be confirmed by the visual observation on the water droplets dyed with methylene blue on the contaminant layer. It is noteworthy that water droplets are always in a hemisphere shape on the diatomite layer when the PDMS is absent in the primer, even the migration time was prolonged to 336 h (Fig. S1 of the SI). The *in-situ* observations in Fig. 1g suggest that water droplets on both the diatomite-covered primer and the uncovered part are in a hemisphere-like shape when the migration time was 0 h. After 72 h, although the water droplet on the uncovered area retains a hemisphere-like shape (Fig. 1h, identified by a yellow circle), it is interesting that the droplet on the diatomite-covered part can already resemble a sphere-like shape (Fig. 1h, marked by red circle). This visual observation has unambiguously confirmed that PDMS plays critical roles in converting the surface wettability of the contaminated layer. As further displayed from Video S1 of the SI, water droplets can easily slide away from the diatomite surface after 72 h of migration . The diatomite powder on the primer was then transferred on a glass slide and flattened for further observation. The fresh diatomite layer (migration time = 0 h, Fig. 1i) allows water droplets to penetrate it due to its inherent superhydrophilicity, whereas a diatomite layer after 72 h of migration allows water droplets to stand on its surface in a sphere-like shape (Fig. 1j, identified by red circle), indicating a conversion from superhydrophilicity to superhydrophobicity.

3.2. Superhydrophobicity transfer property of SH coating

SH surfaces show much greater promise than hydrophobic and hydrophilic surfaces in practical applications for anti-pollution flashover [21, 26, 34]. Herein, silica particles that pre-modified by HMDS were sprayed onto the PDMS-embedded primer to achieve a SH coating. The coating exhibits a mastoid-like hierarchical micro-nano surface structure (Fig. 2a, see also Fig. S2a-c of the SI), an average thickness of 50.28 μm (Fig. S2d of the SI) and a WCA of 157.8^{o} (inset in Fig. 2a). The water droplets casted onto the SH surface can easily bounce away from the SH surface (Video S2 in the SI), confirming a strong water repellent property. Similar with that of SH coating without PDMS, the PDMS-embedded SH coating

exhibits excellent chemical, UV illumination, and thermal stability (Fig. S2e-h and S3 in the SI). The coating surface can maintain its superhydrophobicity after being submerged in extreme corrosion solutions with pH values ranging from 1.0 to 14.0 for 120 hours (Fig. S2e-g in the SI) or exposed to UV irradiation for 168 hours (Fig. S3a of the SI). Test for longer duration indicated that the chemical stability of the SH coating in acidic environment is significantly greater than that in alkaline environment. The coated SH glass slide has lost its SH performance after being submerged in a NaOH solution with a pH of 14.0 for 168 hours (Fig. S2h of the SI). However, the SH surface can retain its SH property even after being submerged in an H_2SO_4 solution with a pH of 1.0 for more than one month (not shown here). The less stability of SH surface against alkaline environment might be due to the slowly but gradually etching of SiO_2 particles in a NaOH solution, which leads to the formation of $NaSiO_3$. Besides, even after annealing at 400°C for two hours, the SH coating that fabricated with 0.9 w% PDMS could still show WCA > 150° and WSA < 10° although the color of the coating changed from milky white to brown (Fig. S3b-f in the SI). Fig. S3g indicates the SH coating without PDMS has lost their SH performance over 300°C, which is in agreement with the thermal stability of most previously-reported methyl groups-modified SH coatings [35, 36]. These results indicate that the unique thermal stability at 400°C is attributed to the presence of PDMS embedded in the resin-based primer.

Diatomite powder was then sieved on the SH surface to track the superhydrophobicity transfer performance of the SH coating. We discovered through an *in-situ* observation that water droplets thrown onto the fresh diatomite layer (i.e., migration time is 0 h) can adsorb the diatomite particles, and the liquid drops easily touch and slide on the SH surface. A closer observation showed that the fresh diatomite particles' inherent superhydrophilic property allowed themselves to enter the water droplets (Fig. 2b, identified by blue circle, see also Video S3 in the SI). When water droplets move over the freshly diatomite-covered SH surface in this scenario, slurry droplets made of diatomite powder and water may form (Fig. 2b, identified by red dashed circle). It is noteworthy that after sufficient migration time, the diatomite

particles were adsorbed on the water droplet's surface rather than absorbing into the water droplet (Fig. 2c, identified by red circle, see also Video S4 of the SI). The diatomite powders were meticulously removed from the SH surface to a cleaned glass slide, and flattened for further observations and WCA test. Again, water droplets can spread and completely penetrate into the fresh diatomite layer due to its intrinsic superhydrophilicity (Fig. 2d, see also Video S5 in the SI). However, in case of the migration time equal to 72 h, the gathered diatomite layer enables water droplets to resident on it in a sphere-like shape (Fig. 2e, identified by red circle) or slide on it while diatomite particles adsorb on the droplet's surface (Video S6 in the SI). We proposed that the diatomite powder has gained SH ability after sufficient migration time. In order to further substantiate the superhydrophobicity transfer effect, the diatomite powders that extracted from the surface of the SH coating were then casted in water to check the wettability (Fig. S4 and Video S7 in the SI). Indeed, wetting phenomenon occurred clearly on the fresh diatomite particles and all the particles rapidly sink in water, whereas the diatomite particles collected after 72 h of migration could float on the water surface due to the outstanding wetting resistance. These observations lead to the development of a model that describes the interactions between water droplets and contaminant particles on a SH surface (Fig. 2f). Clearly, through an *in-situ* observation on the interaction between the water droplets and contaminant particles, this model provides us with some evidence to know whether the superhydrophobicity transfer actually takes place or not.

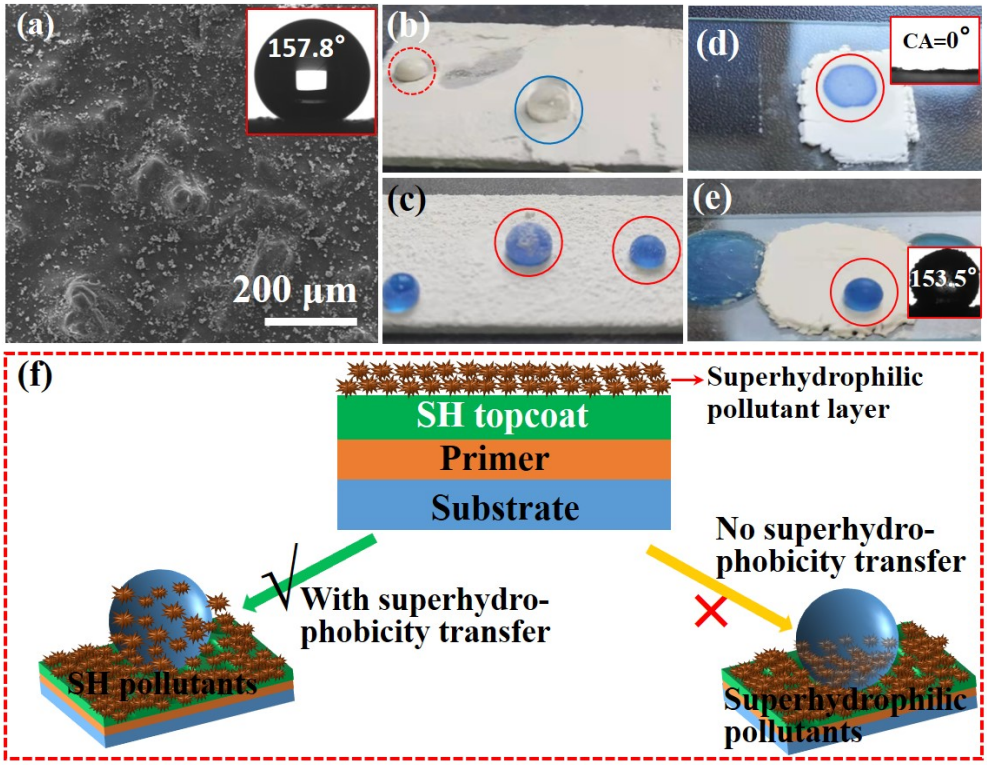

Fig. 2. (a) SEM image of the representative SH coating fabricated in the presence of 0.9 w% PDMS in the primer. (b-c) *In-situ* digital photographs of the PDMS-embedded SH coatings covered by diatomite powder for 0 h (a) and 72 h (b), respectively, together with water droplets. (d-e) Digital photographs of the diatomite layer on glass slides together with water droplets, in which the diatomite powders are removed from the SH surfaces after 0 h (d) and 72 h (e) of migration. (f) A model illustrating the interaction between water droplet and contaminant particles with and without superhydrophobicity transfer effect, respectively.

The evolution of surface wettability of the contaminant layer over the migration time and the PDMS weight percentage (relative to the primer) is shown in Fig. 3a and Fig. S4 of the SI, respectively. We noticed that the SH coating produced without PDMS also showed hydrophobicity transfer effect, which is higher than that of previously reported in SH coating [32]. This performance might be due to the migration of the HMDS residues from the silica-based topcoat, followed by a surface modification. The introduction of PDMS in the primer offers the SH coating a much more powerful superhydrophobicity transfer ability, and

the increasing PDMS amount significantly shortens the migration time that allows the contaminant layer to reach a SH state. As shown in Fig. 3a, it takes 264 h for the WCA on the contaminant layer to reach 145.8° in the absence of HMDS (black curve in Fig. 3a, see more information in Fig. S5 in the SI). However, the diatomite surface has become superhydrophobic with WCA exceeding 150° in 72 h and 48 h of migration when the PDMS weight percents are 0.9% and 1.8%, respectively. There are two periods in the WCA evolution of the specimen in all circumstances during the migration process. The first period (e.g., 0-72 h for 0.9 w% PDMS sample) is the main phase for superhydrophobicity transfer, during which the WCAs of the contaminant layer can be rapidly increased to 150°. Afterwards, the WCAs turned to a steady value, indicating a steady SH state in the second period. The powerful effect of the PDMS amount on the superhydrophobicity transfer performance is further shown by a parallel comparison of the WCAs in Fig. S6, which displays that the WCAs are significantly increased by increasing PDMS fraction in the primer.

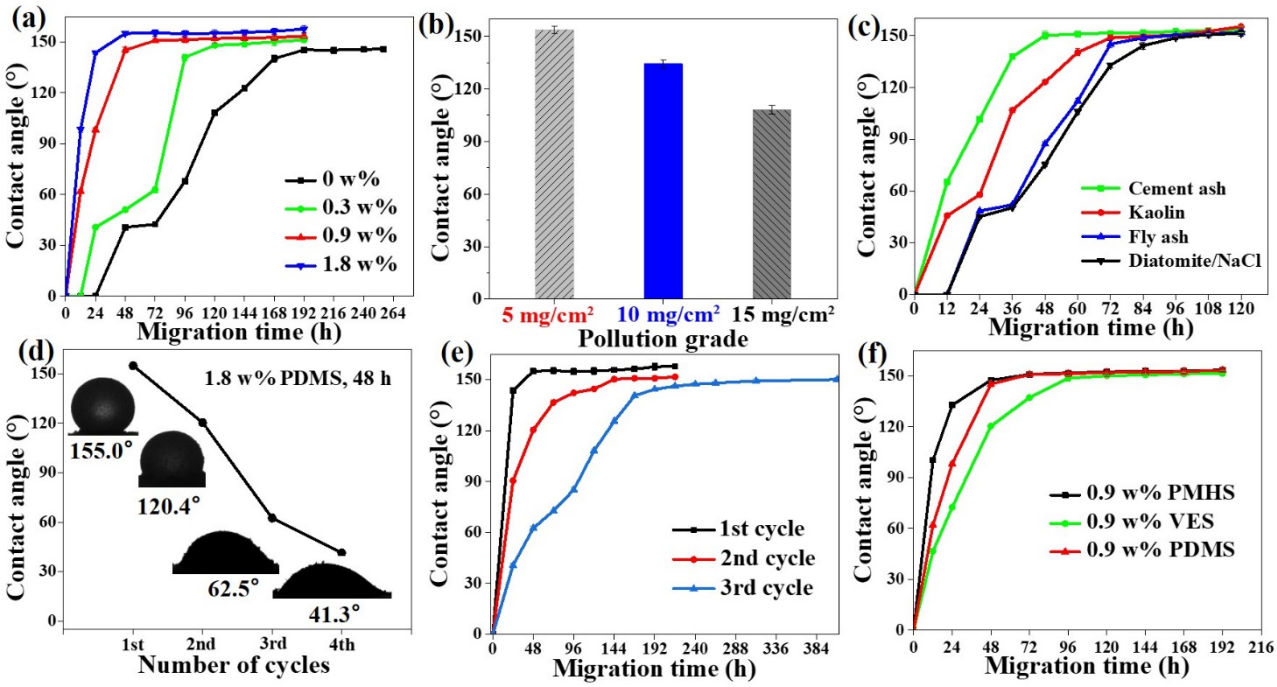

Fig. 3. (a-c) The superhydrophobicity transfer performances of the SH coatings: (a) Evolution of the WCAs on the diatomite layer over migration time; (b) Column chart displayimg the WCAs of the diatomite layer with different pollution grades, in which the migration time is fixed to 72 h; (c) Evolution of the WCAs

over migration time on the surface of different types of simulated contaminants as dictated. (d-e) The superhydrophobicity transfer durability of SH coating with 1.8 w% PDMS: (d) Evolution of the WCAs on the diatomite layer over migration cycles by fixing the migration time as 48 h. (e) Evolution of the WCAs on the diatomite layer over the migration time in different cycles. (f) The superhydrophobicity transfer effect of SH coatings embedded with different migratory reagents.

In addition to the above-discussed migration time and amount of migrating reagent, other variables such as the species of contaminants, temperature, and level of the pollution were also noticed to influence the hydrophobicity transfer performance in a RTV system [37]. It has been noticed that the hydrophobicity transfer process varied considerably depending on the type of polysiloxane and nanoparticle used [33]. Herein, we focus on the impact of the pollution grade, types of contaminants and different migratory reagents on the superhydrophobicity transfer capability in SH coatings. The WCAs of the contaminant layer with various pollutant levels (i.e., light (i.e., 5 mg/cm^2), medium (i.e., 10 mg/cm^2) and heavy (i.e., 15 mg/cm^2)) indicated that the hydrophobicity became lower as the mass of contaminants increase (Fig. 3b). In other words, it takes longer migration time for the contaminants to reach a SH state as the pollutant grade increased. Besides, the effect of different contamination species, including fly ash, cement ash, kaolin, and a diatomite/NaCl mixture, on the superhydrophobicity transfer property is shown in Fig. 3c. The diatomite/NaCl mixture is the pollutant that has the largest hindering effect on the superhydrophobicity transfer, followed by fly ash, kaolin, and cement ash. Cement ash can reach the SH state in 48 h, whereas diatomite/NaCl takes 96 h to do so. The resident water droplets on the various contaminant layers maintain their spherical shape (Fig. S7 in the SI), directly convincing the superhydrophobicity transfer effect.

In order to investigate the durability of the superhydrophobicity transfer capability, the evolution of WCAs over the superhydrophobicity transfer cycles is reported in Fig. 3d-e. By fixing the migration time as 72 h, we noticed that the surface of the diatomite layer cannot reach a SH state after the second cycle, and the WCAs of the diatomite layer decreases with increasing cycle (Fig. 3d). However, the WCAs can

exceed 150° by extending the migration time in each cycle (Fig. 3e). For instance, it takes 48 h, 144 h and 264 h for the contaminant layer surface to reach 155°, 150.3° and 150.7° in the 1st, 2nd and 3rd cycles, respectively. These results indicate that although the migratory chemicals (i.e., PDMS molecules) are consumable, the SH coating displays good superhydrophobicity transfer durability.

As a general protocol, it is of great interest that a SH coating embedded by other migratory organic chemicals such as PMHS and VES also display superhydrophobicity transfer effect. As shown in Fig. 3f, WCAs on the diatomite layer grows with prolonging the migration time in the presence of either PMHS or VES in the primer. We noticed that the SH coating with PMHS displays the highest transfer speed at the early stage of the migration period, in comparison with coatings embedded with HMDS and VES. Then, WCAs on all samples turn to a steady value and the diatomite layer could reach a SH state in sufficient migration time. All of the above-discussed results show that the migration time, pollution species and grade, the migratory species and their amounts all play critical roles in the superhydrophobicity transfer effect of the SH coatings.

3.3. Superhydrophobicity transfer effect of the PDMS-embedded SAP coating

We looked into the performance of the SAP coating embedded with PDMS to present a general protocol for superhydrophobicity transfer effect in SW materials. Water and bean oil repellent micro-nano surface can be produced by spraying fluorocarbon group-modified silica NPs onto the PDMS-embedded resin-based primer (Fig. S8 in the SI). The coating displays a hierarchical micro-nano surface and the thickness is 58.22 μm, slightly higher than that of the SH coating (Fig. S8a-c of the SI). Unlike the methyl groups-modified SH surface, SAP surface have both OCA and WCA higher than 150° (e.g., WCA=165.3°, OCA=156.8°, insets in Fig. S8d of the SI) due to the surface modification by lower surface-energy organic groups (i.e., fluorocarbon groups) compared with the methyl groups. Before and after superhydrophobicity transfer, the behavior of water droplets on the contaminants (i.e., diatomite) resembles that of the above-discussed SH coating system (Fig. 4a-d, identified by blue circles). The *in-situ* digital photographs show

that the bean oil droplets can penetrate into the diatomite layer and touch the original SAP surface, resembling a spherical shape, no matter before and after undergoing the superhydrophobicity transfer (Fig. 4a-b, identified by red circles). As the corresponding diatomite powders are flattened on a glass slide, bean oil droplets completely spread on the contaminant layer (Fig. 4c-d, identified by red circles). Further tests revealed that the OCAs on all the contaminant layers were always 10°, even though the migration time was extended by up to 6 months (not shown here). Unlike the PDMS-absent SH coating that displayed hydrophobicity transfer performance due to the migration of HMDS molecules, the PDMS-absent SAP coating had no any hydrophobicity transfer ability, no matter how long the migration time was. These findings indicate that PDMS plays critical role in the superhydrophobicity transfer process in SAP coating, whereas the fluorocarbon groups that offer SAP property for the coating, are unable to migrate to the contaminant layer to convert the surface to a hydrophobic or oleophobic state.

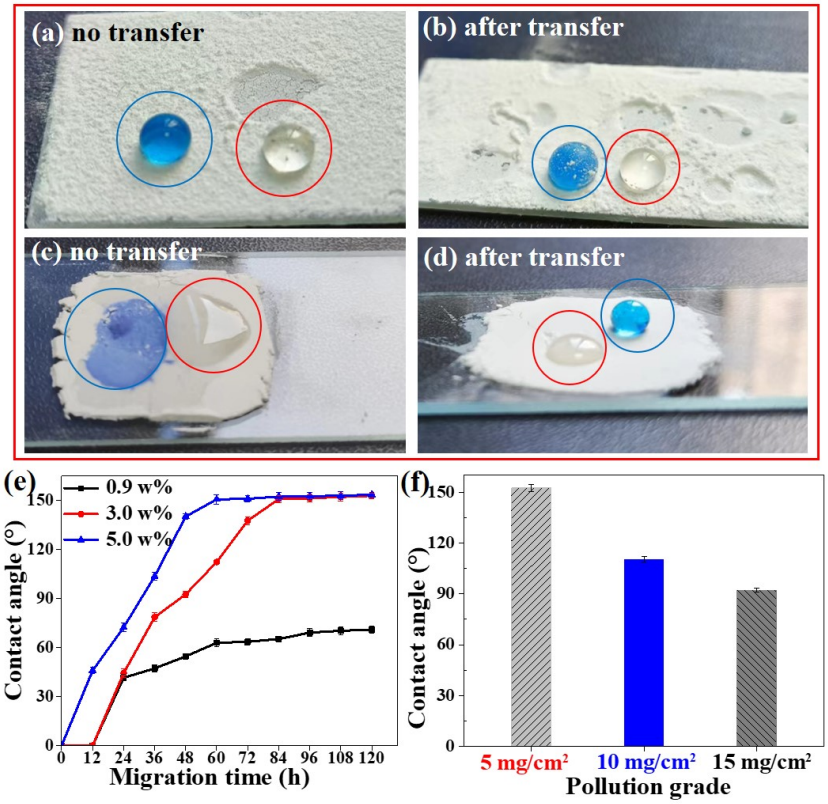

Fig. 4. (a-b) *In-situ* digital photographs of SAP coatings covered by fresh diatomite layer (a) and diatomite after 84 h of migration (b), together with dyed water and bean oil droplets. (c-d) Digital photographs of the diatomite layer on glass slides together with water and bean oil droplets, in which the diatomite powders are removed from the SAP surfaces after 0 h (c) and 84 h (d) of migration. (e) Evolution of the WCAs on the contaminant layer collected at different periods of migration time from SAP coating. The SAP coatings were fabricated in the presence of different PDMS weight percents. (f) The column chart displaying the WCAs on the contaminant layer by simulating light (i.e., 5 mg/cm^2), medium (i.e., 10 mg/cm^2) and heavy (i.e., 15 mg/cm^2) pollution environment, respectively.

The evolution of WCAs on the contaminant layer collected from the PDMS-embedded SAP coating at different periods of migration time (Fig. 4e) are similar to that of SH system. That is, WCAs grow rapidly during the first period, and turn to a steady value in the second period. Besides, higher amount of PDMS caused a growth of the WCA values on the contaminant layers, suggesting a faster superhydrophobicity transfer speed (see also Fig. S9 in the SI). The plot of superhydrophobic transfer for SH and SAP coatings with the same amount of PDMS is depicted in Fig. S10, which clearly displays a significant higher transfer rate of SH coating than that of SAP coating. Additionally, when the migration time is fixed, a heavier pollution level would result in lower WCAs (Fig. 4f). SW

3.4. Mechanism on the superhydrophobicity transfer effect of the superwetting coatings

Based on the aforementioned findings, we infer that the specific migration of low-surface-energy molecules from the coating to the contaminant layer, followed by a surface modification, is what causes the wettability of contaminant layer to change from superhydrophilicity to superhydrophobicity. It was noticed that the solo PDMS-absent primer and the PDMS-absent SAP coating exhibit no noticeable hydrophobicity transfer ability, while the coatings achieved in the presence of PDMS, PMHS and VES display conspicuous superhydrophobicity transfer performance. Besides, the HMDS-incorporated coating showed high hydrophobicity transfer performance even in the absence of PDMS, PMHS and VES.

Therefore, it makes sense that the migratory low-surface-energy species are PDMS, PMHS, VES and HMDS molecules that have been incorporated into the coatings. Among the above-mentioned low surface-free-energy molecules, PDMS, PMHS and VES are much more powerful than HMDS for the superhydrophobicity transfer, which can be confirmed by the fact that the WCAs on the contaminant layer can grow much faster in the presence of PDMS, PMHS and VES. We presumed that migratory groups in the primer (e.g., PDMS, PMHS and VES) are able to migrate more freely than HMDS groups that have been strongly incorporated with silica NPs.

FTIR and XPS analyses of the representative diatomite powders before and after superhydrophobicity transfer were carried out to further reveal the alteration of surface chemical composition of the pollution layer and to get a better insight regarding the related mechanism (Fig. 5a-b). Diatomite powders collected from SAP and SH coatings after superhydrophobicity transfer show new absorption peaks at 2964, 2930 and 2850 cm^{-1} that, in comparison to the FTIR spectrum of the fresh diatomite powder, which can be attributed to the C-H stretching groups [38-41]. Besides, new peak also emerged at around 1264 cm^{-1} in the diatomite collected from SAP coating with sufficient amount of PDMS (red curve in Fig. 5a), which can be indexed to the presence of $(Si\text{-}CH_3)$ groups [42]. Fig. 5b displays the high-resolution XPS spectra of Si (2p) in the fresh diatomite and the diatomite powders that collected from SH coating after superhydrophobicity transfer. In comparison with that of fresh diatomite, the Si (2p) peak of diatomite after superhydrophobicity transfer can be decomposed into two peaks, namely $(CH_3)_3$-Si-O or Si-C (101.5 eV) and -Si-O-Si- (103.4 eV), respectively [43]. Both FTIR and XPS analyses indicate that the diatomite particles have been modified by methyl groups.

Based on the aforementioned results, we can conclude that the unique superhydrophobicity transfer capability of the SW coatings is caused by the migration of low-surface-energy groups (i.e., PDMS, PMHS, VES and HMDS molecules) from the coatings to the contaminant layer, followed by a surface physical or chemical modification (Fig. 5c). We presumed the substantive dynamics behind the migration of low-

surface-energy groups from the primer to the top-coating, and finally to the surface of the contaminant layer, is mainly due to their concentration gradient distribution along the thickness direction of the coating. Similar mechanism has been addressed for a hydrophobicity transfer in RTV system and even in SH coating [33, 37, 44]. For instance, under specific circumstances, lower molecular weight silane chains tend to diffuse to the surface of the pollution layer, increasing the surface hydrophobicity [31, 44, 45]. In a polysiloxane-based SH coating, the ability to transfer hydrophobicity to pollution was linked to the presence of low molar mass polysiloxanes and their diffusion from within to the surface of the material [33, 46].

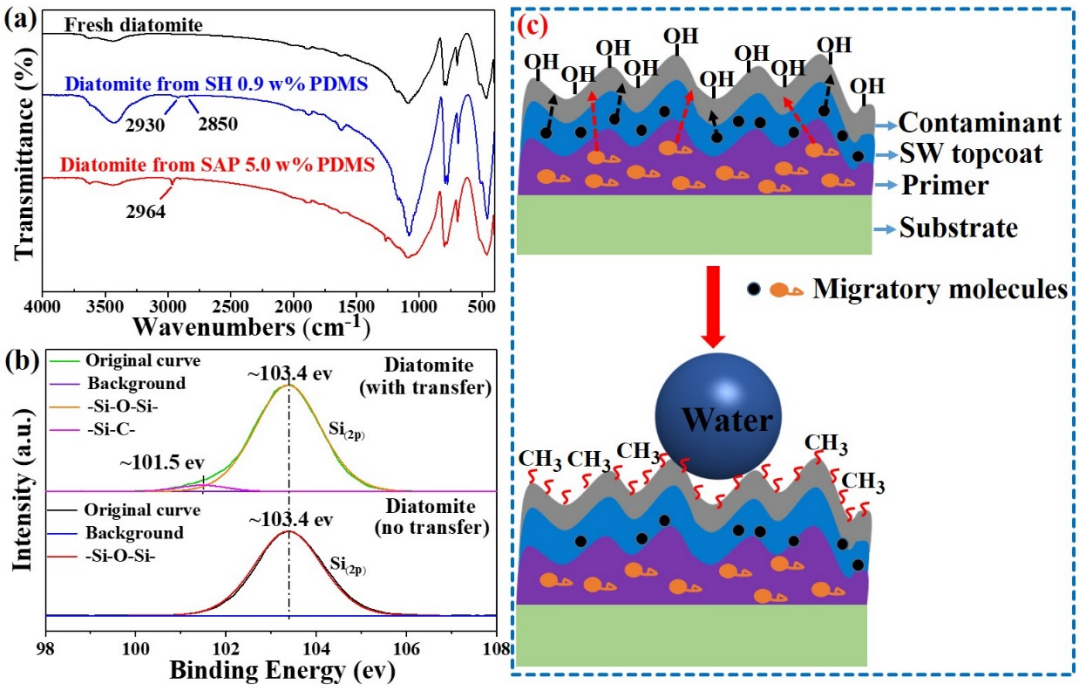

Fig. 5. (a) FTIR spectra of the fresh diatomite (i.e., no superhydrophobicity transfer) and the diatomite powders that collected from SH and SAP coating, respectively, after superhydrophobicity transfer. (b) High-resolution XPS spectra of Si (2p) in the fresh diatomite and the diatomite powders that collected from SH coating after superhydrophobicity transfer. (c) Mechanism behind the superhydrophobicity transfer effect mediated by low-surface-energy migratory molecules (i.e., PDMS, PMHS, VES and HMDS).

For SH materials, biomimetic self-healing or self-repairing is crucial because it gives surfaces good durability after being physically or chemically damaged [47, 48]. One of the strategies to realize self-healing ability is *via* the diffusion or migration of hydrophobic components [46, 49, 50]. Therefore, monitoring the SH surface's capacity for self-healing in our case would enable us to better understand the mechanism behind the superhydrophobicity transfer. Oxygen-plasma was used to treat the PDMS-incorporated SH coating for a self-healing investigation. Upon the plasma treatment for 25 seconds, the WCA on the surface immediately decreased from above 150^{o} in the fresh SH coating to ~0^{o}, causing water droplets to completely spreading the treated part (Fig. S11a, identified by red circle). Comparatively, the portion of the surface without oxygen-plasma treatment kept its SH performance (Fig. S11a, identified by blue circle). It's interesting to note that after storing the oxygen plasma-etched coating under ambient conditions for some time (typically in 24-48 h), the surface wettability could be recovered back to superhydrophobicity (Fig. S11b, identified by dashed red circle, see also the CA image). These findings suggest that low-surface-energy groups were removed during plasma etching, causing the surface to lose its superhydrophobicity (Fig. S11c of the SI). Afterwards, low-surface-energy molecules (typically methyl groups) could then be regained due to the migration of PDMS molecules from the coating to the surface, which would modify the surface and restore its superhydrophobic state. The self-healing performance of the PDMS-incorporated SH coating explains the migration capability of the PDMS molecules and the following surface modification.

3.5. Anti-pollution flashover performance of the SW insulators

After fabricating several representative coated glass insulators, we finally investigate their self-cleaning and anti-pollution flashover characteristics. These specimens included coated SAP and SH insulators, RTV-coated insulator, and hydrophobic resin-based insulator. As shown in Videos S8-S9 in the SI, the representative coated SH insulator outperforms RTV-coated insulator in terms of water repellency and self-cleaning performance. Since the pollution flashover of insulators typically results from the development of

leakage current due to the surface contamination, the outstanding self-cleaning performance undoubtedly facilitates enhancing the anti-pollution flashover ability. Fig. 6a reports the pollution flashover voltages (PFOVs) of the various specimens under a light pollution level, among which the PFOVs of the insulators without superhydrophobicity transfer derived from our previously work [22], are provided for a comparison (grey columns). In each case, the pollution flashover strength with superhydrophobicity transfer effect can be improved. More detailed results and analyses are as follows:

(1) The superhydrophobicity transfer effect slightly improves the anti-flashover ability of the insulator. However, we also noticed that the PFOVs of SAP and SH insulator before and after superhydrophobicity transfer are comparable. The SAP and SH specimens display 75.728 and 72.002 kV of PFOVs after 168 h of migration, which are only 3.2% and 4.6%, respectively, higher than those of the corresponding specimens without superhydrophobicity transfer. The excellent self-cleaning performance provided by the original SH surfaces plays a critical role in antifouling performance. With or without superhydrophobicity transfer, the condensation of water drops would slide off from the 15° tilted insulator surface under gravity, taking away the contaminants and consequently improving the anti-flashover ability of the insulator.

(2) SH and SAP insulators after superhydrophobicity transfer has shown significant enhancement of anti-flashover strength in comparison with RTV insulator. For details, the PFOVs of the SH and SAP insulators are 15.59% and 21.58%, respectively, higher than that of the RTV insulator. This noticeable difference is due to the self-cleaning property of the SH and SAP surfaces. However, both the initial RTV surface and the contaminant layer on RTV gain no SH state even after storing the specimens for 168 h. Consequently, condensation of water leads to a gradual growing and adhering of water droplets to the RTV surface, which reduces the PFOVs. Indeed, as shown in Fig. 6b-d, the SH and SAP insulators' surfaces were clean after the PFOV test, while the RTV insulator still had pollutant residues and a tiny quantity of water drops on it. It has been noticed that the strong water repellency ability of a surface facilitated to expanding the clean area on the surface, lengthening the insulation channel and enhancing insulation strength [17]. Furthermore,

significantly fewer pollutants on SH and SAP insulators than on RTV surface, which is due to the excellent anti-pollution characteristic [19, 29], contributes to the improvement of pollution flashover strength.

(3) It was noteworthy that the PDMS-embedded resin-based hydrophobic insulator has greatly improved its anti-flashover capacity after superhydrophobicity transfer. The PFOV after 168 h of migration can reach 69.068 kV, which is 17.9% higher than that of the PDMS-absent resin-based insulator. This is ambiguously due to the superhydrophobicity transfer effect. As demonstrated in the previous sections, the contamination layer on the PDMS-embedded resin-based coatings has gained SH performance after sufficient migration time, repelling water droplets away from the contaminant surface and thereby improving the anti-flashover strength.

All of these findings show that creating SH and SAP coatings with superhydrophobicity transfer effect facilitates improving the anti-pollution flashover strength, and thus are eminently suited for anti-pollution flashover of electrical devices in heavy contamination environments.

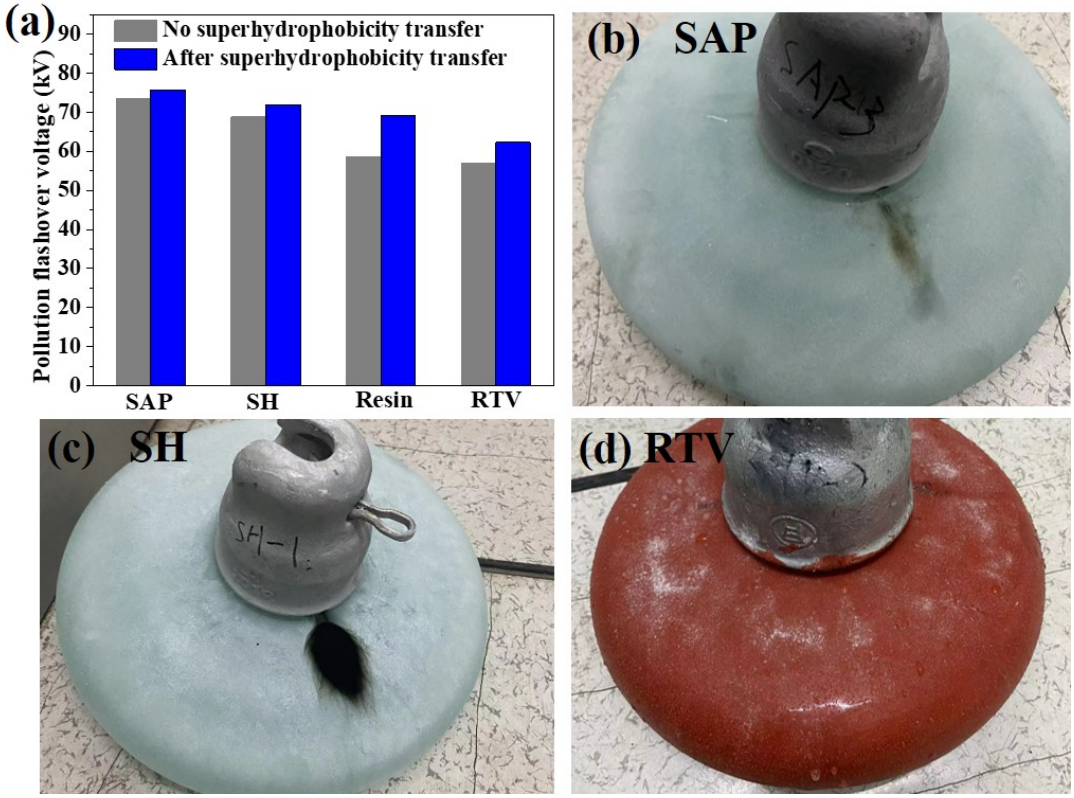

Fig. 6. Pollution flashover voltages (PFOVs) with (blue column chart) and without (grey column chart) superhydrophobicity transfer of coated SAP, SH, RTV, hydrophobic (i.e., coated with only PDMS-embedded resin-based primer) glass insulators. The PFOVs without superhydrophobicity transfer are from the data we previously reported [22]. (b-d) Digital photographs of the representative coated glass insulators after pollution flashover test.

4. Conclusions

By embedding low-surface-energy species such as PDMS, PMHS, VES and HMDS in SW coatings, we developed a facile methodology to realize a superhydrophobicity transfer effect in AW coatings. The low-surface-energy molecules can migrate either from the primer to the topcoat and finally to the contamination layer or directly from the topcoat to the contamination layer when the SW surface is stained by simulated pollutants such as diatomite, fly ash, cement ash, kaolin, and a mixture of diatomite/NaCl. The migration

of low-surface-energy molecules followed by the surface modification on the pollutant particles leads to the unique conversion of the contaminant layer's wettability from superhydrophilicity to superhydrophobicity. The superhydrophobicity transfer performance of the SW coatings was affected by the migration time, pollutant species and grade, and the types and amount of the migratory reagents . Lower pollution grade and higher fraction of migratory reagents promote the superhydrophobicity transfer rate. In particular, superhydrophobicity transfer effect can improve the anti-pollution flashover strength of the coated SH or SAP glass insulators. The SH and SAP insulators with superhydrophobicity transfer effect display 3.2% and 4.6% PFOVs higher than the corresponding insulators without superhydrophobicity transfer, and 15.59% and 21.58% higher PFOVs than that of the RTV insulator, respectively. Besides, the PFOV of the PDMS-embedded resin-based hydrophobic insulator after superhydrophobicity transfer is 17.9% stronger than that of the resin-based insulator without migratory reagent. The presented protocol provides a novel insight for fabricating SW coatings with not only liquid-repellent surfaces but also superhydrophobicity transfer property, which is promising in practical anti-pollution flashover in power network systems.

CRediT authorship contribution statement

Chuxiong Qiu, and Wei Xiong: Synthesis, Data analysis, Processed figures, Investigation, Writing - original draft. Helong Zhang, Rong Zhang, and Shengwu Wang: Characterizations, Data curation. Arnauld Robert Tapa, Albert Trokourey, Weibing Zhou: Writing - re-view & editing. Junwu Chen, Lee Li, and Zhi Chen: Conceptualization. Yi Xie, Ivan P. Parkin and Xiujian Zhao: Supervision, Conceptualization, Methodology, Validation, Project administration, Writing - review & editing. All authors have given approval to the final version of the manuscript.

Declaration of competing interest

The authors declare that they have no known competing financial interests or personal relationships that could have appeared to influence the work reported in this paper.

Data availability

Data will be made available on request.

Acknowledgements

This work is supported by the Overseas Expertise Introduction Project (111 project) for Discipline Innovation of China (Grant No. B18038).

References

[1] M. Tzianou, G. Thomopoulos, N. Vourdas, K. Ellinas, E. Gogolides, Tailoring wetting properties at extremes states to obtain antifogging functionality, Adv. Funct. Mater., 31 (2021) 2006687.
[2] L.-B. Zhang, H.-X. Zhang, Z.-J. Liu, X.-Y. Jiang, S. Agathopoulos, Z. Deng, H.-Y. Gao, L. Zhang, H.-P. Lu, L.-J. Deng, L.-J. Yin, Nano-silica anti-icing coatings for protecting wind-power turbine fan blades, J. Colloid Interface Sci., 630 (2023) 1-10.
[3] G. Zhao, G. Zou, W. Wang, R. Geng, X. Yan, Z. He, L. Liu, X. Zhou, J. Lv, J. Wang, Competing Effects between Condensation and Self-Removal of Water Droplets Determine Antifrosting Performance of Superhydrophobic Surfaces, ACS Appl. Mater. Inter., 12 (2020) 7805-7814.
[4] Z. Liu, F. Feng, Y. Li, Y. Sun, K. Tagawa, A corncob biochar-based superhydrophobic photothermal coating with micro-nano-porous rough-structure for ice-phobic properties, Surf. Coat. Tech., 457 (2023) 129299.
[5] T. Zhang, J. Deng, L.-Z. Zhang, A photothermal self-healing superhydrophobic coating with anti-frosting and anti-corrosion properties, Prog. Org. Coat., 180 (2023) 107569.
[6] K. Yang, J. Shi, L. Wang, Y. Chen, C. Liang, L. Yang, L.-N. Wang, Bacterial anti-adhesion surface design: surface patterning, roughness and wettability: a review, J. Mater. Sci. Technol., 99 (2022) 82-100.
[7] W. Xiong, L. Li, F. Qiao, J. Chen, Z. Chen, X. Zhou, K. Hu, X. Zhao, Y. Xie, Air superhydrophilic-superoleophobic SiO_2-based coatings for recoverable oil/water separation mesh with high flux and mechanical stability, J. Colloid Interface Sci., 600 (2021) 118-126.
[8] S. Kareem, Y. Xie, T. Li, Y. Ding, E.A. Tsiwah, A.S.A. Ahmed, J. Chen, F. Qiao, Z. Chen, X. Zhao, Base-catalyzed synthesis of superhydrophobic and antireflective films for enhanced photoelectronic applications, J. Mater. Res. Technol., 9 (2020) 3958-3966.
[9] Y. Hu, S. Kareem, H. Dong, W. Xiong, S. Tian, J. Shamsi, L. Li, X. Zhao, Y. Xie, $CsPbBr_3@SiO_2$ core-shell nanoparticle films for superhydrophobic coatings, ACS Appl. Nano Mater., 4 (2021) 6306-6315.
[10] J. Zhang, J. Wei, B. Li, X. Zhao, J. Zhang, Long-term corrosion protection for magnesium alloy by two-layer self-healing superamphiphobic coatings based on shape memory polymers and attapulgite, J. Colloid Interface Sci., 594 (2021) 836-847.

[11] L. Zhang, X. Liu, J. Yan, Z. Li, S. Huang, Y. Weng, J. Li, C. Yuan, P. Han, S. Ye, X. Zhang, Preparation of superhydrophobic coating with anti-corrosion and anti-fouling properties on the surface of low manganese steel by electrodeposition, Surf. Coat. Tech., 460 (2023) 129412.
[12] G. Zhu, J. Su, C. Yin, H. Li, Y. Yao, L. Zhang, X. Yao, X. Zhang, F.-Q. Liu, Constructing a robust ZIF-7 based superhydrophobic coating with the excellent performance in self-cleaning, anti-icing, anti-biofouling and anti-corrosion, Appl. Surf. Sci., 622 (2023) 156907.
[13] X. Shen, T. Mao, C. Li, F. Mao, Z. Xue, G. Xu, A. Amirfazli, Durable superhydrophobic coatings based on CNTs-SiO2gel hybrids for anti-corrosion and thermal insulation, Prog. Org. Coat., 181 (2023) 107602.
[14] B. Tao, L. Cheng, J. Wang, X. Zhang, R. Liao, A review on mechanism and application of functional coatings for overhead transmission lines, Front. Mater., 9 (2022).
[15] Arshad, G. Momen, M. Farzaneh, A. Nekahi, Properties and applications of superhydrophobic coatings in high voltage outdoor insulation: A review, IEEE Trans. Dielectr. Electr. Insul., 24 (2017) 3630-3646.
[16] H. Jin, P. Jin, R. Niu, Y. Li, B. He, N. Gao, H. Zhang, Flashover characteristics of discrete water droplets on the surface of super-hydrophobic silicone rubber, IEEE Trans. Dielectr. Electr. Insul, 21 (2014) 1718-1725.
[17] Y. Li, H. Jin, S. Nie, P. Zhang, N. Gao, Dynamic behavior of water droplets and flashover characteristics on a superhydrophobic silicone rubber surface, Appl. Phys. Lett., 110 (2017) 201602.
[18] J. Chen, J. Chen, L. Li, S. Wang, Y. Xie, Study on the self-cleaning phenomenon and anti-pollution flashover performance of micro-nanostructure superhydrophobic coating surface under a high humidity environment, Colloids Surf., A, 630 (2021) 127552.
[19] W. Xu, J. Niu, K. Tian, Z. Huang, J. Li, F. Wang, Y. Wei, Y. Zhao, Enhanced pollution flashover of a slurry coalescence superhydrophobic coating, IEEE Trans. Dielectr. Electr. Insul., 28 (2021) 310-317.
[20] S. Wang, Q. Zou, X. Zhao, J. Chen, L. Li, J. Chen, Y. Xie, K. Yang, Predicting the DC pollution flashover voltage on the insulation surfaces with superhydrophobicity, Colloids Surf., A, 646 (2022) 128987.
[21] M.-X. Zhu, H.-G. Song, J.-C. Li, J.-Y. Xue, Q.-C. Yu, J.-M. Chen, G.-J. Zhang, Superhydrophobic and high-flashover-strength coating for HVDC insulating system, Chem. Eng. J., 404 (2021) 126476.
[22] Y. Xie, W. Xiong, S. Kareem, C. Qiu, Y. Hu, I.P. Parkin, S. Wang, H. Wang, J. Chen, L. Li, Z. Chen, H. Sun, X. Zhao, Robust superamphiphobic coatings with gradient and hierarchical architecture and excellent anti-flashover performances, Nano Res., 15 (2022) 7565-7576.
[23] J. Li, Z. Jing, F. Zha, Y. Yang, Q. Wang, Z. Lei, Facile spray-coating process for the fabrication of tunable adhesive superhydrophobic surfaces with heterogeneous chemical compositions used for selective transportation of microdroplets with different volumes, ACS Appl. Mater. Interfaces., 6 (2014) 8868-8877.
[24] J. Li, Y. Wei, Z. Huang, F. Wang, X. Yan, Z. Wu, Electrohydrodynamic behavior of water droplets on a horizontal super hydrophobic surface and its self-cleaning application, Appl. Surf. Sci., 403 (2017) 133-140.
[25] S. Ren, S. Wang, Z. Dong, J. Chen, L. Li, Dynamic behaviors and self-cleaning property of droplet on superhydrophobic coating in uniform DC electric field, Colloids Surf., A, 626 (2021) 127056.
[26] S. Liu, S. Liu, Q. Wang, Z. Zuo, L. Wei, Z. Chen, X. Liang, Improving surface performance of silicone rubber for composite insulators by multifunctional nano-coating, Chem. Eng. J. , 451 (2023) 138679.
[27] A. Allahdini, G. Momen, F. Munger, S. Brettschneider, I. Fofana, R. Jafari, Performance of a nanotextured superhydrophobic coating developed for high-voltage outdoor porcelain insulators, Colloid Surface A, 649 (2022) 129461.

[28] P. Parand, M. Mohammadi, A.A. Shayegani Akmal, M. Samadpour, M. Dehghani, E. Parvazian, Sequential RTV/(TiO_2/SiO_2) nanocomposite deposition for suppressing the leakage current in silicone rubber insulators, Appl. Phys. A, 126 (2020) 333.
[29] H. De Santos, M.Á. Sanz-Bobi, Research on the pollution performance and degradation of superhydrophobic nano-coatings for toughened glass insulators, Electr. Power Syst. Res., 191 (2021) 106863.
[30] Y. Liu, Y. Guo, B. Wang, X. Zhang, G. Huang, G. Zhang, Y. Liu, Q. Deng, G. Wu, Pollution morphology characteristics on a superhydrophobic surface and its pollution flashover voltage in DC electric field, High Volt., 7 (2022) 564-574.
[31] X. Wen, X. Yuan, L. Lan, L. Hao, Y. Wang, S. Li, H. Lu, Z. Bao, RTV silicone rubber degradation induced by temperature cycling, Energies., 10 (2017) 1054.
[32] G. Chen, J. Chen, Y. Xie, L. Li, Z. Chen, Study on hydrophobic substances transfer in superhydrophobic anti-pollution flashover insulating material, Insulating Material, 53 (2020) 25-29.
[33] A.C. Ribeiro, B.G. Soares, J.G.M. Furtado, A.A. Silva, N.S.S.E. Couto, Superhydrophobic nanocomposite coatings based on different polysiloxane matrices designed for electrical insulators, Prog. Org. Coat., 168 (2022) 106867.
[34] M. Zhu, J. Xue, Y. Wei, G. Li, G. Zhang, Review of interface tailoring techniques and applications to improve insulation performance, High Volt., 7 (2022) 12-31.
[35] C. Hu, W. Chen, T. Li, Y. Ding, H. Yang, S. Zhao, E.A. Tsiwah, X. Zhao, Y. Xie, Constructing Non-Fluorinated Porous Superhydrophobic SiO_2-Based Films with Robust Mechanical Properties, Colloids Surf., A., 551 (2018) 65-73.
[36] S.-C. Cha, E.K. Her, T.-J. Ko, S.J. Kim, H. Roh, K.-R. Lee, K.H. Oh, M.-W. Moon, Thermal stability of superhydrophobic, nanostructured surfaces, J. Colloid Interface Sci., 391 (2013) 152-157.
[37] Z. Jia, H. Gao, Z. Guan, L. Wang, J. Yang, Study on hydrophobicity transfer of RTV coatings based on a modification of absorption and cohesion theory, IEEE Trans. Dielectr. Electr. Insul., 13 (2006) 1317-1324.
[38] Y. Qing, S. Shi, C. Lv, Q. Zheng, Microskeleton-Nanofiller Composite with Mechanical Super-Robust Superhydrophobicity against Abrasion and Impact, Adv. Funct. Mater., 30 (2020) 1910665.
[39] Z. Chen, F. Li, L. Hao, A. Chen, Y. Kong, One-step electrodeposition process to fabricate cathodic superhydrophobic surface, Appl. Surf. Sci., 258 (2011) 1395-1398.
[40] X. Zhou, S. Yu, S. Guan, Z. Lv, E. Liu, Y. Zhao, Fabrication and characterization of superhydrophobic TiO_2 nanotube coating by a facile anodic oxidation approach, Surf. Coat. Tech., 354 (2018) 83-91.
[41] T. Li, Y. Ding, S. Kareem, F. Qiao, G. Ali, C. Ji, X. Zhao, Y. Xie, Hexamethyldisilazane-triggered room temperature synthesis of hydrophobic perovskite nanocrystals with enhanced stability for light-emitting diodes, J. Colloid Interface Sci., 552 (2019) 101-110.
[42] A. Rashid, M. Amin, M. Ali, A. Khattak, Aging exploration of long term multistressed HTV-silicone rubber/silica/alumina composites for high voltage insulation, Mater. Res. Express, 5 (2018) 095301.
[43] Q. Gao, J. Hu, R. Li, L. Pang, Z. Xing, L. Xu, M. Wang, X. Guo, G. Wu, Preparation and characterization of superhydrophobic organic-inorganic hybrid cotton fabrics via γ-radiation-induced graft polymerization, Carbohyd. Polym., 149 (2016) 308-316.
[44] R. Sarathi, M. Danikas, RTV silicone rubber coatings for outdoor insulators: a concise review of some factors affecting their behavior and some comments, J. Eng. Sci. Technol. Rev., 14 (2021) 163-169.
[45] D.A. Swift, C. Spellman, A. Haddad, Hydrophobicity transfer from silicone rubber to adhering pollutants and its effect on insulator performance, IEEE Transactions on Dielectrics and Electrical Insulation, 13 (2006) 820-829.

[46] F.Z. Kamand, B. Mehmood, R. Ghunem, M.K. Hassan, A. El-Hag, L. Al-Sulaiti, A. Abdala, Self-healing silicones for outdoor high voltage insulation: mechanism, applications and measurements, Energies 15 (2022) 1677.
[47] Z. Wang, D. Yao, Z. He, Y. Liu, H. Wang, Y. Zheng, Fabrication of durable, chemically stable, self-healing superhydrophobic fabrics utilizing gellable fluorinated block copolymer for multifunctional applications, ACS Appl. Mater. Interfaces, 14 (2022) 48106-48122.
[48] Q. Li, X. Zhang, S. Ben, Z. Zhao, Y. Ning, K. Liu, L. Jiang, Bio-inspired superhydrophobic magnesium alloy surfaces with active anti-corrosion and self-healing properties, Nano Res., 16 (2023) 3312-3319.
[49] A.C.C. Esteves, Y. Luo, M.W.P. van de Put, C.C.M. Carcouët, G. de With, Self-replenishing dual structured superhydrophobic coatings prepared by drop-casting of an all-in-one dispersion, ACS Appl. Mater. Interfaces, 24 (2014) 986-992.
[50] H. Zhou, H. Wang, H. Niu, A. Gestos, T. Lin, Robust, self-healing superamphiphobic fabrics prepared by two-step coating of fluoro-containing polymer, fluoroalkyl silane, and modified silica nanoparticles, Adv. Funct. Mater., 23 (2013) 1664-1670.